THE JOURNAL OF NAVIGATION (2018), **71**, 467–481.
doi:10.1017/S0373463317000649

Statistical Analysis of the Detection Probability of the *TianTuo-3* Space-based AIS

Shiyou Li, Lihu Chen, Xiaoqian Chen, Yong Zhao and Lei Yang

(*College of Aerospace Science and Engineering, National University of Defense Technology, Changsha, 410073, China*)
(E-mail: toneylab@163.com)

The Micro-Nano satellite *TianTuo-3* (TT-3) developed by the National University of Defense Technology (NUDT) was successfully launched on 20 September 2015. The space-based Automatic Identification System (AIS) on board TT-3 works well and stably receives AIS signals from global vessels. In this work, we perform statistical analysis on the detection probability of the vessels in the concerned areas by using the TT-3 AIS data. The results suggest that the detection probability of vessels decreases as the distribution density increases, especially in the offshore areas of dense traffic and the TT3-AIS vessel detection probability in the oceans can be higher than 40%, indicating that the TT-3 AIS has achieved a high probability of coverage of vessels for a single receiving antenna. The analysis results will present helpful references both in evaluating the potential application of satellite-based AIS and for designing the next generation space-based AIS which might greatly improve the detection probability of ocean-going vessels.

KEYWORDS

1. TianTuo-3. 2. Space-based AIS. 3. Detection probability. 4. Signal confliction.

Submitted: 14 January 2017. Accepted: 13 August 2017. First published online: 14 September 2017.

1. INTRODUCTION. Using the Self-Organised Time Division Multiple Access (SOTDMA) communication protocol (International Telecommunication Union (ITU), 2001), the universal vessel-borne Automatic Identification System (AIS) (Graveson, 2004; Cairns, 2005) is a vessel-to-vessel and vessel-to-shore (and vessel-to-space) reporting system in which ships broadcast short fixed-length Time Division Multiple Access (TDMA) messages including static and dynamic messages and voyage information for the purpose of collision avoidance, pilot scheduling and spatial awareness to assist in navigation decisions. AIS information can be used for dynamic tracking, automatic exchange of ship identification, position, course, speed and other navigational information (Silveira et al., 2013). Combining communications, network and information technology, AIS is both a navigational aid and a safety information system.

The coverage range of terrestrial AIS is limited by Very High Frequency (VHF) radio propagation ranges, typically around 35–40 Nautical Miles (NM). To overcome this shortcoming, space-based AIS has been developed in the last few years (Wahl and Høye, 2003). A space-based AIS system can cover a much larger area than a traditional AIS system and uses satellite-based receivers to realise much wider range AIS signal detection. Since 2003, space-based AIS has been extensively researched (Eriksen et al., 2006; Cain and Meger, 2009; Tobehn et al., 2011; Cervera et al., 2011; Carson-Jackson, 2012; Høye et al., 2008). It is possible to monitor a wide maritime area using satellites equipped with AIS receivers. In civil applications, space-based AIS has achieved space tracking, monitoring civil vessels and logistics regulation (Eriksen et al., 2006). In military applications, the wider ranged AIS signals can greatly improve military vessels' accuracy of interpretation by combining with satellite imagery technology, and thus the space-based AIS technology is of important strategic significance by improving the positioning accuracy, accurately determining the target attributes and auxiliary target screening and so on (Carthel et al., 2007; Chaturvedi et al., 2012).

Satellites equipped with high sensitivity AIS receivers are powerful tools and the technology has attracted great interest from many countries and organisations. With respect to AIS satellite or payload development, the United States (US) (e.g. Duffey et al., 2008; Vu Trong et al., 2011), Norway (e.g. Eriksen et al., 2006; Narheim et al., 2011), Canada (e.g. Cain and Meger, 2009; Brusch et al., 2010), Germany (e.g. Holsten, 2009), Luxembourg (e.g. Burzigotti et al., 2012), and China (e.g., Chen et al., 2015; Cheng et al., 2014, 2015), as well as some other countries and organisations, have launched their own AIS satellites or AIS payloads. China successfully launched its first AIS Nano-satellite *TianTuo-1* (Chen et al., 2015; Cheng et al., 2014, 2015), which was developed by the National University of Defense Technology (NUDT), on 10 May 2012. Subsequently, NUDT developed its third Micro-Nano satellite series, *TianTuo-3* (Li et al., 2017a; 2017b), which is a constellation, carrying a new generation space-based AIS receiver as one of the most important main payload elements.

The *TianTuo-3* was successfully launched into a solar synchronous orbit at a height of 496 km on 20 September 2015. *TianTuo-3* is a constellation including one main satellite *LvLiang-1* (weight 23 kg), one mobile satellite *Smart* (weight 1 kg) and four Femto-satellites *Stardust 1-4* (weight 0·1 kg). The AIS receiver is one of the main payloads on board *LvLiang-1*, hereafter called *TianTuo-3* AIS or TT3-AIS or TT3-AIS receiver. Several types of new technologies were applied in designing the TT3-AIS receiver, including multi-channel technology, Doppler frequency shift estimation compensation technology, receiving antenna optimisation technology, and so on, with respect to the first AIS Nano-satellite *TianTuo-1* in China (Chen et al., 2015; Cheng et al., 2014, 2015). As a result, the TT3-AIS has partly solved the signal conflict problems and thus the *TianTuo-3* greatly improves the signal detection ability. During the debugging stage (20 September – 20 December 2015), the TT3-AIS worked smoothly in orbit, receiving effective AIS messages every day. Daily averaged messages ranged from 20,000 to 40,000 (Li et al., 2017b). *TianTuo-3* had been working for more than seven months up until the end of the data used for this study (30 April 2016).

The TT3-AIS receiver was designed to use four frequency channels to receive AIS messages. Two of frequency channels use frequency points at 161·975 MHz and 162·025 MHz (ITU, 2010), which are the official frequencies promulgated by the ITU for the traditional AIS system (ITU, 2001). The other two frequency channels at 156·775 MHz and

https://doi.org/10.1017/S0373463317000649 Published online by Cambridge University Press

156·825 MHz have been applied for by the International Maritime Organization (IMO) from the ITU and are particularly used for long-ranged communication for the space-based AIS receiver and maritime vessels (refer to Rec. ITU-R M.1371-4 (ITU, 2010)). The two new frequency channels receive AIS message type 27 for scheduled position reports. This is similar to types 1, 2 and 3. For the receiving characteristics, receiving ability, and data formats of the TT-3 AIS receiver, one can refer to our previous work (Li et al., 2017b).

It is important for maritime authorities to track, classify and monitor the movement of vessels in order to track their voyage history in their area of jurisdiction. For a Low Earth Orbit (LEO) satellite space-based AIS, the coverage area, or field of view, of the satellite is around 2,880 NM in diameter, which corresponds to a high number of SOTDMA cells. This means that many ships within the field of view are visible to the satellite, which causes AIS messages from multiple vessels to be received simultaneously within the same slot period by the satellite. This prevents decoding of the AIS messages. As a result, some vessels may not be detected by the space-based AIS receiver.

It is necessary to investigate the detection probability of a satellite of space-based AIS. The detection probabilities of space-based AIS can be defined as the ratio of the number of ships detected by the space-based AIS to the number of all the vessels in the coverage area and the detection probability is an important performance index. The pursuit of higher and higher detection probabilities is one of the important aims of developing space-based AIS.

Little published research has studied the detection probabilities of space-based AIS. The innovative *TianTuo-1,* successfully launched into space in May 2012, was estimated to have a ship detection probability of about 30% (Cheng et al., 2015). It was reported that during the testing phase of the AIS satellite *ExactView-1*, it resulted in detection rates of up to 15%–40% better than any of the previous satellite sensors (ExactEarth, 2013).

In this paper, we will not address the technology and the data format of AIS, but will study the detection probability of TT-3 AIS of the vessels in some areas of dense traffic and in the global oceans by utilising the AIS data received over the seven months from launch to 30 April 2016.

2. STATIC SNAPSHOT DISTRIBUTION OF THE GLOBAL VESSELS AND COVERAGE ANALYSIS OF THE TT3-AIS RECEIVER.

2.1. *Dataset.* In this section we will use two types of dataset for analysis. The first is combined AIS data within a time interval from 08:20 UT on 22 January to 20:00 UT on 23 January 2016 obtained from one commercial company, and it is termed as dataset "S". The second one AIS data obtained from the TT3-AIS receiver over the same time interval and is termed dataset "T". The dataset S is made by integrating the shore-based AIS receiving network and the current running AIS satellites. It is reasonable to recognise the completeness of dataset S in the current condition since the dataset S is the most comprehensive data obtained under existing conditions. In this paper, we suggest that dataset S contains all vessels which are equipped with AIS transmitters.

The commercial company provides a data service for users mainly by continuous monitoring of the vessel, so the original data is at a high temporal resolution. Furthermore, in addition to vessels' Maritime Mobile Service Identity (MMSI) number, position, speed and turning rate, and other basic information, S also includes much additional information for detailed description to the vessels, such as the type of ship, the length of the ship, draft

https://doi.org/10.1017/S0373463317000649 Published online by Cambridge University Press

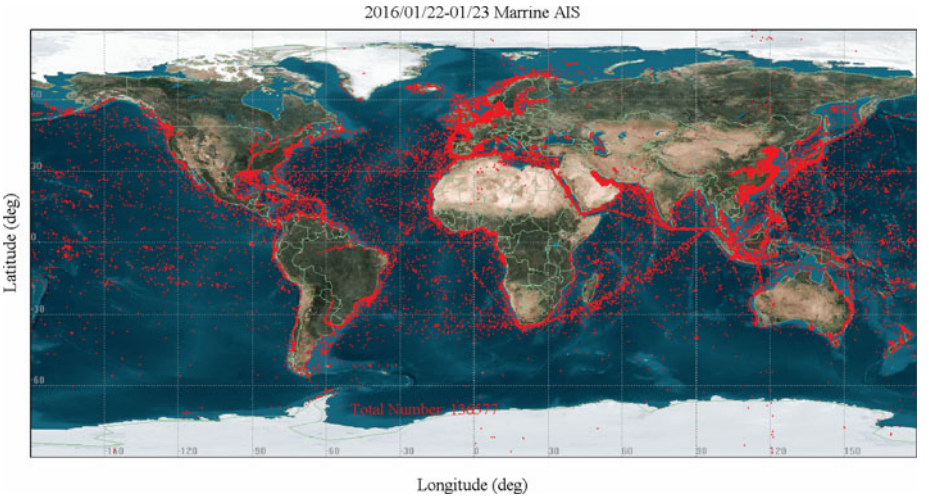

Figure 1. Static distribution of global vessels obtained from dataset S2. Dataset S2 was formed by combining the shore-based AIS data network and the AIS satellite observation networks within the observation time interval of 08:20 UT on 22 January to 20:00 on 23 January 2016. This represents all vessels globally, with a total number of 136,577.

depth and so on. Thus, dataset S occupies more than six gigabytes and is too large to process. In processing, only one small portion of the data is read and processed to remove the duplicate MMSI messages and the redundant information, saving the most important information in the AIS data in one processing circle. By repeating the reading, removing, and saving process, a compact dataset (termed S1) is formed, which contains some information useful in this work, including the vessel's MMSI number and the corresponding location, speed and other information. The dataset S1 occupies a space of less than one megabyte, which will greatly facilitate the subsequent file operation.

2.2. *Snapshot distribution of global vessels and Coverage of TT-3 AIS.* Over two days, the changing of position of ships can be neglected since the movement of ships is usually slow. The time factor in the data is no longer considered, thus duplicated MMSI numbers can be removed during the two days and a simplified dataset S2 is finally obtained. The dataset S2 represents a statistical snapshot distribution of global vessels sailing worldwide on the ocean. The total number is 136,577. Figure 1 shows the static distribution of global vessels obtained from dataset S2. It is clear that in some economically developed regions, such as east Asia, western Europe, north America and other economically active areas, offshore vessels are densely distributed. There are also many vessels distributed on the main sea-route channels, including the "East Asia, Indian Ocean, West Asia, Mediterranean, Western Europe channel" and the "East Asia, Indian Ocean, Cape of Good Hope, the Atlantic, Western Europe or North America" channel. In deep oceanic regions, vessels have a relatively sparse distribution except for those in the sea-route channels.

Similar to the creation of dataset S2 from S, the TT-3 AIS dataset T can be simplified by removing the duplicated MMSIs over the same time interval (08:20 UT 22 January – 20:00 UT 23 January 2016). Thus, a new dataset can be obtained and is termed dataset T1 which represents a snapshot distribution of global vessels using the TT-3 AIS receiver.

https://doi.org/10.1017/S0373463317000649 Published online by Cambridge University Press

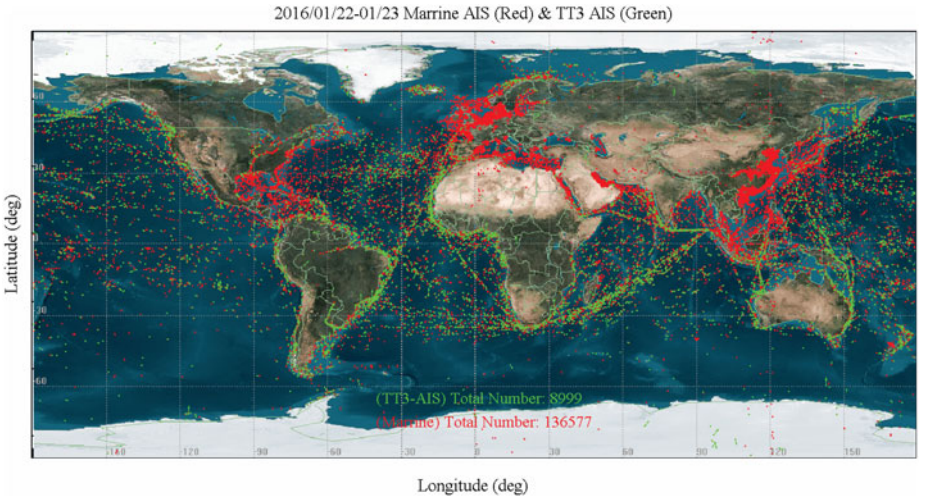

Figure 2. Epoch global overlaid distribution of the vessels obtained from the data set S2 (red, representing all the ships on the sea at that time) and the dataset T1 (green, received by the TT3-AIS) within the time interval 08:20 UT 22 January – 20:00 UT January 2016.

Epoch analysis is performed and the dataset S2 and T1 are overlaid in Figure 2, showing the distribution of global vessels from these two datasets. Points in red and green respectively represent the vessels from datasets S2 and T1. Note that because of the overlap between green and red, most of the green points have red points at the same time. As shown in Figure 2, the number of vessels in dataset T1 is 8,999, accounting for only 6·59% of the number in dataset S2. This result suggests that only a small portion of the global vessels can be detected by the TT-3 AIS. However, it should be noted that most of the un-received vessels are close to the coastline in the areas of dense traffic. For example, in east Asia offshore, the Mediterranean and Middle East offshore and the southeast offshore regions of middle-north America, the T1 dataset yields an apparently low coverage rate by the TT3-AIS receiver.

However, it is clear that in the deep oceanic region there are higher coverage rates. Detailed analysis will be carried out in the next section.

3. STATISTICAL ANALYSIS OF DETECTION PROBABILITY.

3.1. *Grid detection probability.* A space-based AIS system could have signal links with a much larger number of vessels within its field of view than the traditional ship-to-ship or ship-to-shore AIS system. Thus, many ships within the field of view will cause AIS messages to be received simultaneously by the satellite thereby preventing decoding of the AIS messages, which will result in signal conflict. As a result, some vessels may not be detected. The detection probabilities of space-based AIS (P_{AIS}) can be defined as the ratio of the number of ships detected by the space-based AIS (N_{AIS}) to the number of all the vessels in the coverage area (N_{all}), i.e., $P_{AIS} = N_{AIS}/N_{all}$. However, this approach is somewhat controversial and there are different opinions on obtaining the value of N_{all}.

Skauen (2016) has developed a general method to estimate the tracking capability of space-based AIS sensors for the results obtained by AISsat-1 and AISsat-2. Based on

https://doi.org/10.1017/S0373463317000649 Published online by Cambridge University Press

data gathered over a 15-day period by AISSat-1 and AISSat-2, Skauen's work (Skauen, 2016) has studied the tracking capability of the space-based AIS system. The results are based only on the data recorded by the space-based AIS sensors themselves. The tracking capability was expressed as:

$$TC_{MMSI}(grid\ cell) = \frac{N_{det}^{MMSI}(grid\ cell)_{T_{start}}^{T_{end}}}{N_{tot}^{access}(grid\ cell)_{T_{start}}^{T_{end}}} \tag{1}$$

where, $N_{det}^{MMSI}(grid\ cell)_{T_{start}}^{T_{end}}$ and $N_{tot}^{access}(grid\ cell)_{T_{start}}^{T_{end}}$ respectively, represent the number of space-based AIS systems accessing the grid cell in which an MMSI was detected within a specified timeframe and the total number of space-based AIS system accesses to the grid cell over the specified timeframe between T_{start} and T_{end}.

However, in our work, since the dataset S2 can be regarded as the aggregation of all the AIS Class-A vessels, the total number in each grid cell can be obtained by S2, and the detection probability of the TT3-AIS can be simplified to $P_{AIS,c} = N_{AIS,c}/N_{all,c}$, where $N_{AIS,c}$ and $N_{all,c}$ respectively, represent the number of MMSIs seen by TT3-AIS in a specified grid cell during a specified time period and the total number of MMSIs (given by S2) in the same grid cell during the same time period. The time range for analysis in this section is set to be the same time interval (08:20 UT 22 January 2016 – 20:00 UT 23 January 2016) as it is in Section 2.1. This is a different approach and is more straightforward than that used by Skauen (2016).

The size of each grid cell is $2^\circ \times 2^\circ$ and thus the Earth surface is divided into 90×180 grid cells. In each grid cell, the $N_{AIS,c}$ is accumulated from each vessel passing the grid cell during the time span of dataset S2 and T1 by removing the duplicated MMSI. Thereafter, the detection probabilities can be obtained. Figure 3 shows the total vessel distribution of $N_{all,c}$ in the grid cells of $2^\circ \times 2^\circ$, representing the total MMSI in the grid cell obtained by S2. The scale of the colour bar in Figure 3 represents the numbers of vessels in each grid cell. The distribution of vessels in grid cells is similar to the results shown in Figure 1, suggesting that there are several offshore sea regions, e.g., east Asia, western Europe, north America and other economically active areas, in which the vessels are densely distributed.

It might be worth pointing out that a $2^\circ \times 2^\circ$ grid cell covers a smaller and smaller geographic area as one moves further away from Equator to the north or south poles, so that the vessel density corresponding to a given number of ships within the cell increases with the distance from the Equator. For instance, a grid cell with 100 ships at 60°N has a larger vessel density than a grid cell with 100 ships that is close to Equator. Thus, a geographic factor g_c must be considered in evaluating the vessel density worldwide.

Suppose the northern hemisphere has been divided into 45 belts from the equator to the northern pole by a delta degree of 2°. So, the area of the belts can be obtained by:

$$ds = 2\pi R_E^2 \cos\omega \cdot (\Delta\omega) \tag{2}$$

and the area factor is:

$$f_{ds} = \cos\omega \cdot (\Delta\omega) \tag{3}$$

To be convenient, the geographic factor is defined as: $g_c = f_{ds}/f_{ds|\omega=0}$. We have $\omega = \pi \cdot \theta/180$ and $\Delta\omega = \pi \cdot \Delta\theta/180$, where $\theta \in [0, 90)$ and $\Delta\theta = 2$.

Thus, the geographic factors can be obtained. Take the first belt at the equator for example, $g_c = 1$. Other typical values are: when $\theta = 10^\circ$, $g_c = 0{\cdot}9848$; when $\theta = 30^\circ$,

https://doi.org/10.1017/S0373463317000649 Published online by Cambridge University Press

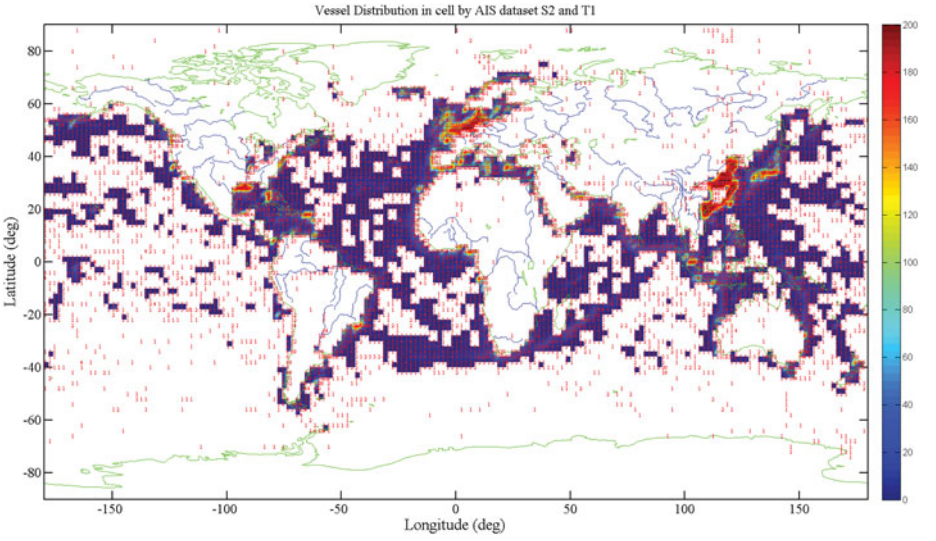

Figure 3. Regional distribution of global vessels in the 2° × 2° grid cells.

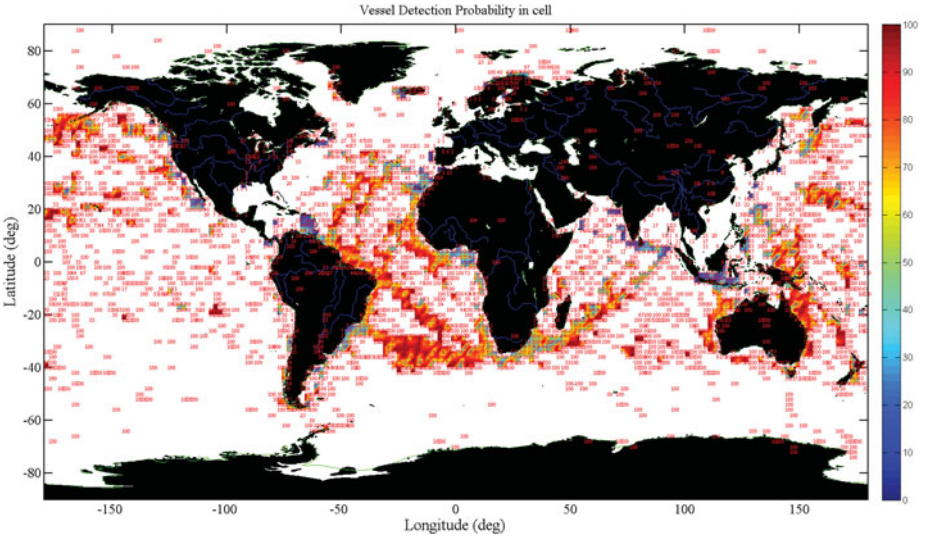

Figure 4. Detection probability of TT3-AIS to the global vessels in the 2° × 2° grid cells.

g_c = 0.8660; when θ = 60°, g_c = 0·5; and when θ = 88°, g_c = 0·0349. However, the geographic factor g_c has no impact on the detection probability ($P_{AIS,c} = N_{AIS,c}/N_{all,c}$), so we will not take it in the next subsection.

Similarly, Figure 4 plots the detection probability of TT3-AIS for global vessels during the same time span according to datasets S2 and T1 obtained by the formula $P_{AIS,c} = N_{AIS,c}/N_{all,c}$ in the 2° × 2° grid cells. In Figure 4, the scale in the colour bar represents the detection probability. As is shown in Figure 4, the detection probability is much higher in

https://doi.org/10.1017/S0373463317000649 Published online by Cambridge University Press

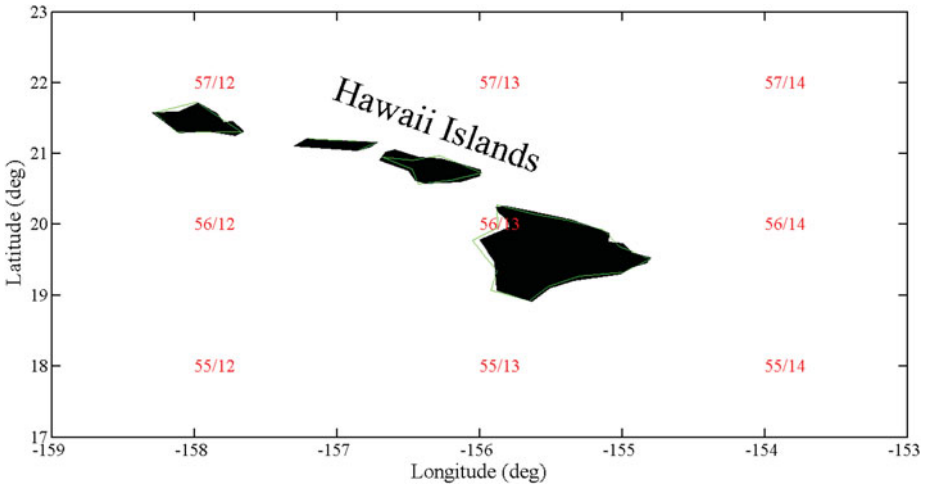

Figure 5. Example of grid cell denotation for C_i^j, showing the main island of Hawaii, where i = 56, j = 13.

the deep oceanic regions than in close offshore regions. Note that it is proportional with the coverage rates as shown in Figure 2. In the sparsely distributed regions, the detection probability of TT3-AIS for vessels in the corresponding grid cell is 100%. However, in the densely distributed regions, such as east Asia, western Europe, north America and other economically active areas, the detection probability is much lower, and even down to 0%. In the following subsection, we will study the detection probability regionally.

3.2. *Regional analysis.* As can be seen from Figure 2, the detection probability of TT3-AIS is very low in many areas offshore. In this section, we will perform detailed analysis for the vessel distribution and the detection probability of TT3-AIS by dividing the global oceans and seas into several regions on the basis of the two datasets S2 and T1.

The areas of dense traffic include: (1) the South China Sea, (2) the Mediterranean, (3) the Red Sea, (4) the Persian Gulf, (5) the western and northern European offshore areas, (6) the middle-north America offshore area and (7) the northeast Asia offshore area. The three main oceanic regions are: (8) the Pacific Ocean, (9) the Atlantic Ocean and (10) the Indian Ocean. The detection probability in these regions will be detailed.

As shown in Section 3.1 and in Figure 4, the Earth surface has been compartmentalised into a grid of 90×180 $2^\circ \times 2^\circ$ cells. For the convenience of study, the grid cells will be numbered by C_i^j in the present work, where the subscripts i and j respectively denote the sequence number in the latitude direction and in the longitude direction. For example, the grid cell at which the main island of Hawaii is located can be numbered as C_{56}^{13} as is shown in Figure 5. The grid cells' inclusion in each sub-region will be defined first. Taking the Mediterranean for example as shown in Figure 6, the geographical longitude-latitude range of the Mediterranean is roughly [30, 44, −5, 35] without excluding the land area. Thus the grid cells within it include C_i^j with $\mathrm{i} \in \{[62, 67]\}$ and $\mathrm{j} \in \{[91, 97]\}$ except for several grid cells over the land.

Similarly, the inclusion of grid cells in the other sub-regions can also be defined. In this subsection, we mainly perform analysis on the statistics of the detection probabilities of TT3-AIS for the vessels within areas of dense traffic.

https://doi.org/10.1017/S0373463317000649 Published online by Cambridge University Press

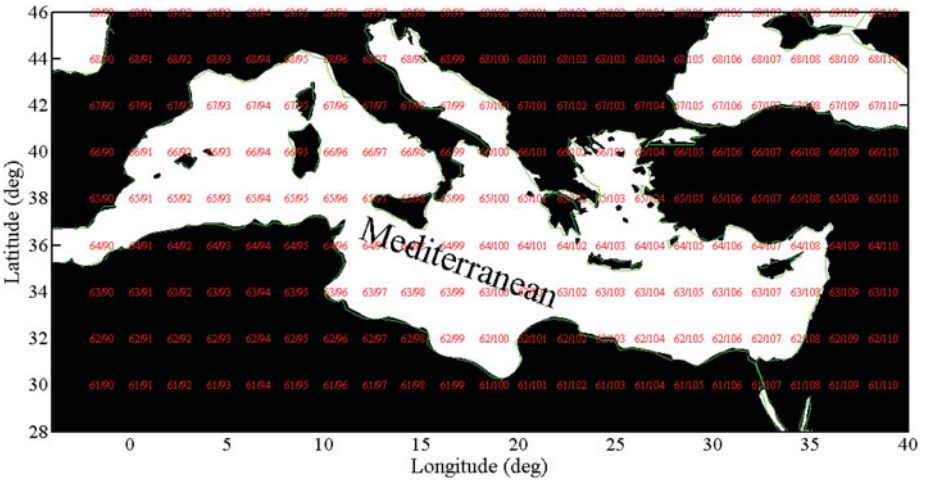

Figure 6. Example of sub-region for study, showing the inclusion of grid cells for the Mediterranean.

Table 1. Detection probability of TT3-AIS described by $P_{AIS,\max}(subregion)$ $P_{AIS,aver}(subregion)$ $P_{AIS,region}(subregion)$, and for dataset T1 in the seven areas of dense traffic.

No.	Sub-region	$P_{AIS,\max}$ (%)	$P_{AIS,aver}$ (%)	$P_{AIS,region}$ (%)
1	South China Sea	25	14·44	0·05
2	Mediterranean	9	3·82	0·14
3	Red Sea	16·67	11·38	3·93
4	Persian Gulf	4·55	2·76	0·83
5	North Europe	33·83	11·08	2·19
6	America Offshore	100	19·2	2·26
7	Northeast Asia Offshore	100	25	0·75
8	Pacific Ocean	100	73·93	44·14
9	Atlantic Ocean	100	73·56	57·10
10	Indian Ocean	100	79·86	54·66

The detection probability in the previously defined sub-regions can be described by the following three variables. The first is the maximal detection probability in grid cells within the regions, $P_{AIS,\max}$. The second is the grid-cell-averaged value of the $P_{AIS,c}$, i.e., $P_{AIS,aver}$ and the last is the total detection probability within the corresponding region $P_{AIS,region}$. These variables are defined as:

$$P_{AIS,\max} = \max(P_{AIS,c}(c_i^j)) \tag{4}$$

$$P_{AIS,aver} = \mathrm{mean}(P_{AIS,c}(c_i^j)) \tag{5}$$

$$P_{AIS,region} = \frac{\sum N_{AIS,c}(c_i^j)}{\sum N_{All,c}(c_i^j)} \tag{6}$$

The results are shown in Table 1 which lists the geographical division of the regions and the corresponding detection probability described by the three variables $P_{AIS,\max}$, $P_{AIS,aver}$ and $P_{AIS,region}$. It can be seen that from Table 1, that $P_{AIS,\max}$ (column 2) in

https://doi.org/10.1017/S0373463317000649 Published online by Cambridge University Press

the America Offshore and Northeast Asia Offshore areas equals 100% because in some grid cells within the corresponding region, vessels are sparsely distributed and will be detected by TT3-AIS, while the $P_{AIS,aver}$ and $P_{AIS,region}$ are rather low. Thus, the $P_{AIS,\max}$ is not suitable to describe the detection probability for the whole region but just for a reference.

From $P_{AIS,aver}$ the detection probabilities only reach 14·44%, 3·82%, 11·38%, 2·76%, 11·08%, 19·2% and 25% respectively in the seven areas of dense traffic. A similar conclusion can also be made from $P_{AIS,region}$. It can be seen that the detection probability of TT3-AIS is very low in the most concerning regions which might be caused by severe signal conflict since the distribution of vessels in these regions are very dense as shown in Figure 1. The totally averaged detection probability of the seven regions is less than 5%. However, for the grid-cell-averaged detection, probability reaches 73·93%, 73·56% and 79·86% respectively in the Pacific Ocean, the Atlantic Ocean and the Indian Ocean, and the total averaged detection probability can be as high as 44·14%, 57·10% and 54·66%. The results in the oceanic regions are better than those in the published works. For example, the detection rates were up to 15%–40% as was reported that during the testing phase of the AIS satellite *ExactView-1* (ExactEarth, 2013).

It is necessary to explain why $P_{AIS,region}$ is so much smaller than $P_{AIS,aver}$ in Table 1. For example, suppose that there are six grid cells in one region, in which the total numbers of $N_{all,c}$ are respectively 4, 4, 44, 10, 16, 922, while the detected numbers of $N_{AIS,c}$ are respectively 1, 1, 0, 1, 2, 0. Thus the results of the detection probabilities in the grid cells are 25%, 25%, 0%, 10%, 12·5% and 0%. So, one can see that the maximum is 25%, the average is 12·1% and the total is 0·5%. As a result, the grid cells with very low detection probabilities are the ones that have many vessels, and they therefore contribute strongly to the $P_{AIS,region}$.

3.3. *Statistical analysis.* In this subsection, the detection probability of the TT-3 AIS for vessels in areas of dense traffic is statistically studied by using the TT-3 AIS data from its launch to 30 April 2016.

Although the dataset S2 is obtained from AIS over two days, it represents the static distribution of the global vessels. Therefore, the static distribution is in a quasi-static state and the dataset S2 can be employed for the basis of calculating the detection probability even for data obtained on other days.

TT3 had been working normally for about six months up to 30 April 2016. Except for the periods of testing, the TT3-AIS receiver could receive AIS signals normally. In the test phase, 40,000 messages were received by the satellite per day (Li et al., 2017b). The orbit of TT3 is sun-synchronous with an inclination angle of 97·5° and the orbit altitude is 496 km, so the orbit period is 94·5 minutes. Due to the rotation of the Earth, the projection of the ground track of the satellite moves 15° westward every cycle and 1,670 km equivalently in the equatorial plane. The swath width of the TT3-AIS receiving antenna is 2,250 km, so that the coverage area of the TT3-AIS receiver on the ground can join seamlessly. The TT3-AIS can cover any point on the Earth at least twice during one solar day. Therefore, one solar day is selected as the unit to analyse the AIS detection probability in the present statistical study.

Similar to the work reported in Section 3.2, the TT3-AIS messages are extracted for one solar day and this then forms dataset Ti, where "i" represents the day unit. As for the data in dataset T1, the distribution in each grid cell can also be obtained and thus the three variables for each dataset Ti can be evaluated.

https://doi.org/10.1017/S0373463317000649 Published online by Cambridge University Press

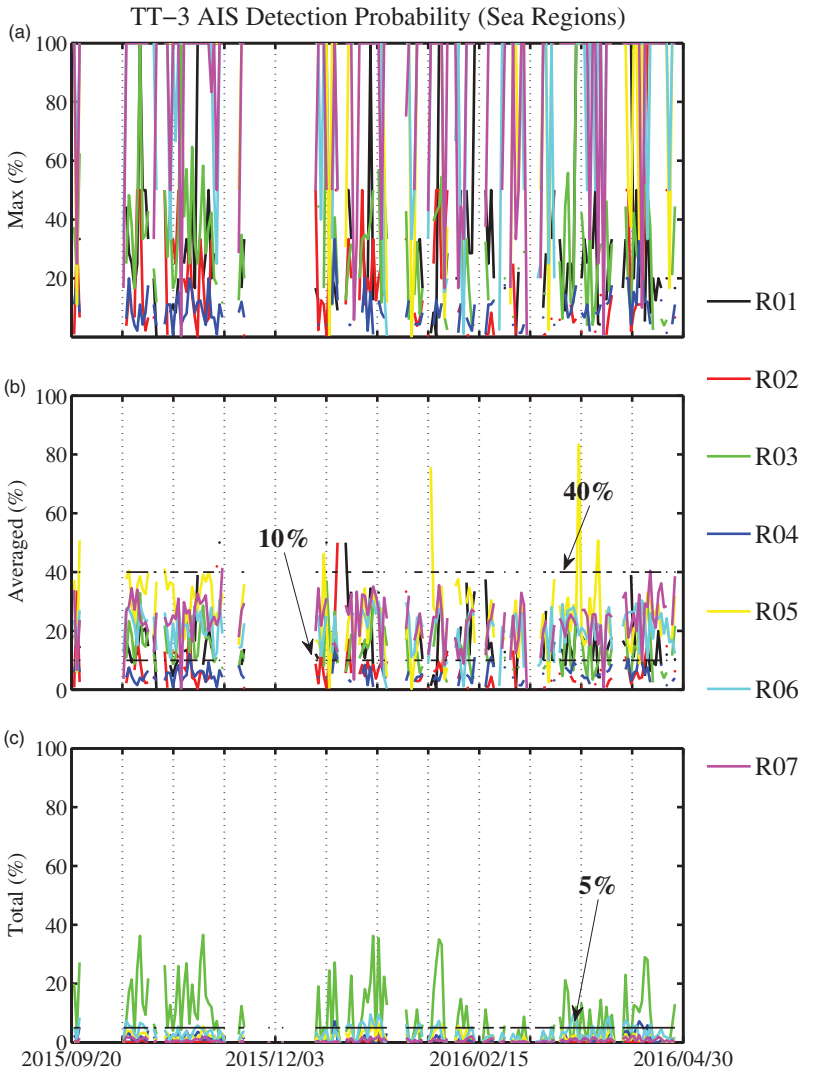

Figure 7. Detection probability of TT3-AIS described by $P_{AIS,\max}$, $P_{AIS,aver}$ and $P_{AIS,region}$ for dataset Ti in the seven areas of dense traffic. R01 (in black): South China Sea; R02 (in red): Mediterranean; R03 (in green): Red Sea; R04 (in blue): Persian Gulf; R05 (in yellow): North Europe; R06 (in cyan): America Offshore; R07 (in magenta): Northeast Asia Offshore.

Figures 7 and 8 plot the results, showing the detection probabilities in the seven areas of dense traffic (Figure 7) and those in the oceanic regions (Figure 8). The first panel in both figures plots the $P_{AIS,\max}$; the second panel plots the $P_{AIS,aver}$ and the last one the $P_{AIS,region}$. The curves in different colours represent the detection probabilities in different regions as denoted in the denotation under the figure. In each panel, the horizontal axis represents the date.

The TT3-AIS did not work continuously over 24 hours due to the influence of other factors such as other test tasks. Thus, the actual work time was not the same on different dates. Even so, a relatively stable detection probability in each region can be seen in Figure 7.

https://doi.org/10.1017/S0373463317000649 Published online by Cambridge University Press

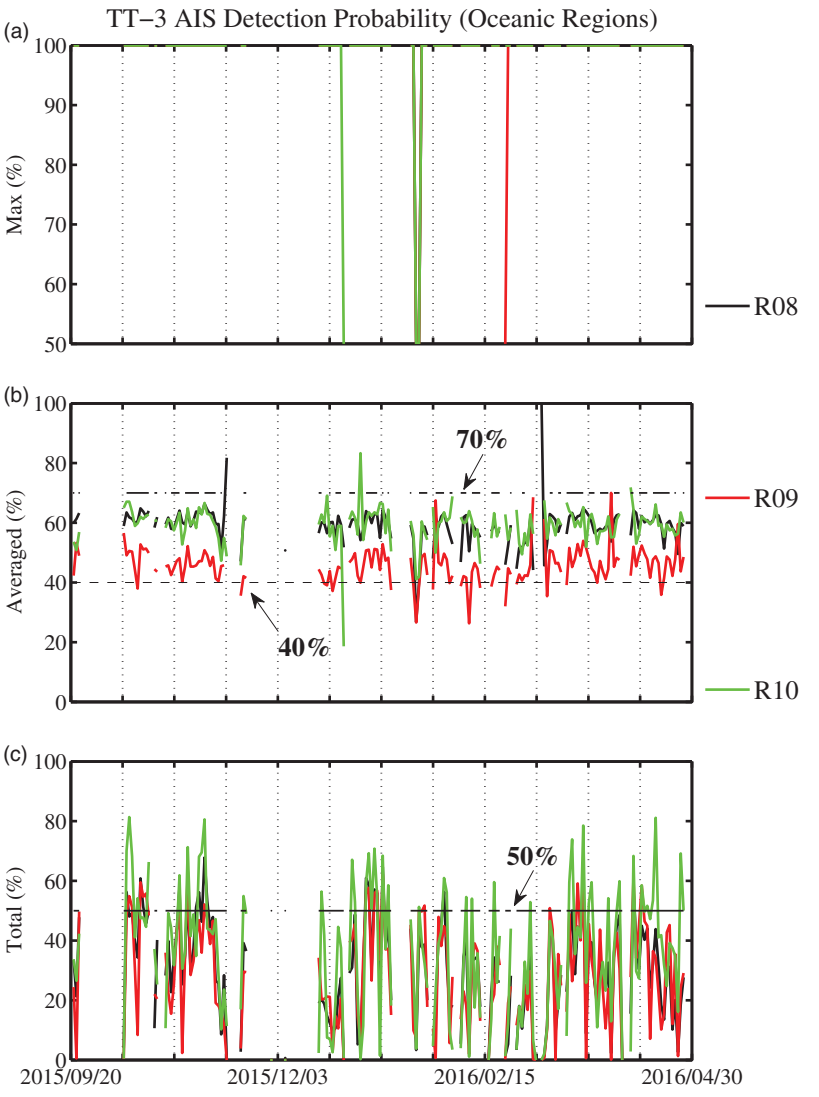

Figure 8. Detection probability of TT3-AIS described by $P_{AIS,\max}$, $P_{AIS,aver}$ and $P_{AIS,region}$ for dataset Ti as in Figure 7 for the three oceanic regions in right column, including R08 (in black): the Pacific Ocean; R09 (in red): the Atlantic Ocean; R10 (in green): the Indian Ocean.

For example, the grid-cell-averaged detection probability in the areas of dense traffic, i.e., $P_{AIS,aver}$ is stably below 40% as denoted by the horizontal line in Figure 7(b), and $P_{AIS,region}$ is mainly below 5% denoted by the line in Figure 7(c). In the oceanic regions, $P_{AIS,aver}$ is stably between 40% and 70% as shown in Figure 7(e), while it ranges from low value to about 50%.

The TT3-AIS worked smoothly after its launch on 20 September 2015. It is useful to evaluate the averaged probabilities for the areas of dense traffic both from the grid-cell-averaged detection probabilities and from the totally detection probabilities. The results are listed in Table 2.

https://doi.org/10.1017/S0373463317000649 Published online by Cambridge University Press

Table 2. Statistics of the averaged detection probability of TT3-AIS described by the $P_{AIS,aver}$ and the $P_{AIS,region}$ for dataset Ti in the seven areas of dense traffic.

No.	Sub-region	Average of $P_{AIS,aver}$ (%)	Average of $P_{AIS,region}$ (%)
1	South China Sea	16·2	0·04
2	Mediterranean	7·8	0·14
3	Red Sea	14·3	8·7
4	Persian Gulf	5·4	1·19
5	North Europe	25·3	1·78
6	America Offshore	20·5	3·01
7	Northeast Asia Offshore	23·4	0·67
8	Pacific Ocean	58·9	29·36
9	Atlantic Ocean	45·7	28·16
10	Indian Ocean	59·2	35·35

It should be pointed out that the numbers in Table 2 vary from the corresponding ones in Table 1. Take $P_{AIS,region}$ in the Atlantic Ocean for example, it is smaller in Table 2 (28·16%) than that in Table 1 (57·10%). This is because the numbers in Table 2 are the statistically averaged total. However, the trend and relevant numbers of the statistical results in Table 2 are similar to those in Table 1. This is coherent to the stabilities as shown in Figure 7. In the areas of dense traffic as listed in Table 2, the grid-cell-averaged detection probability of TT3-AIS generally range from 5% to 25%, while it is rather small for the totally averaged detection probabilities in these regions. It exhibits extremely tiny values in the totally averaged detection probabilities especially in the South China Sea (0·04%), the Mediterranean (0·14%) and Northeast Asia Offshore (0·67%), suggesting extremely severe signal conflicts in receiving AIS messages in these regions.

4. CONCLUSION AND DISCUSSION. The main purpose of this paper is to perform a statistical study on the coverage and the detection probability of the TT3-AIS in some areas of dense traffic and oceans with the data received within the time interval from its launch (20 September 2015) to 30 April 2016. Firstly, the global static distribution of vessels was obtained by analysing the integrated AIS data which is merged into commercial AIS data from shore-based and space-based AIS. Secondly, the world was graphically divided into several sub regional units and then merged into the following seven areas of dense traffic and three oceanic regions: (1) the South China Sea, (2) the Mediterranean, (3) the Red Sea, (4) the Persian Gulf, (5) the western and northern European offshore, (6) the middle-north America offshore and (7) the northeast Asia offshore; (8) the Pacific Ocean, (9) the Atlantic Ocean, and (10) the Indian Ocean. Based on the commercial AIS dataset S2, the vessel distribution and the detection probability of TT3-AIS in the areas of dense traffic and oceanic regions were studied. Finally, statistical analysis of the detection probability to the global vessels as well as those in the concerned areas was performed by using the daily TT3-AIS data from TT-3's launch on 20 September 2015 to 30 April 2016.

The conclusions can be summarised as follows:

- The global static distribution of vessels is rather dense in the near-offshore regions; however, the vessels are relatively sparsely distributed in the ocean regions except for those in the sea-route channels.

https://doi.org/10.1017/S0373463317000649 Published online by Cambridge University Press

- The detection probability of vessels decreases as the distribution density increases, especially in the offshore regions such as the South China Sea, the Mediterranean and the Northeast Asia Offshore area, where the vessels are rather concentrated. In these regions, the total averaged detection probabilities are extremely tiny (less than 1%), suggesting extremely severe signal conflicts in receiving the AIS messages in these regions.
- In the oceanic regions, the grid-cell-averaged detection probability reaches 73·93%, 73·56% and 79·86% respectively in the Pacific Ocean, the Atlantic Ocean and the Indian Ocean, and the totally averaged detection probability can be as high as 44·14%, 57·10% and 54·66%. The detection probability of TT3-AIS for vessels in the oceans can be more than 40%, indicating that the TT-3 AIS has achieved a great probability of coverage of vessels in the oceans considering there is only a single receiving antenna on board the TT-3 satellite. The results in the oceanic regions are better than those in the published works, for example, the detection rates were up to 15%–40% as was reported during the testing phase of the AIS satellite *ExactView-1* (ExactEarth, 2013).

In this work we have also calculated that in most of the oceanic grid cells as shown in Figure 4, Table 1 and Table 2, the detection probabilities can be 100%, similar to those predicted by Eriksen et al. (2006; 2010) and Høye et al. (2008).

The analysed results will present helpful references both in evaluating the potential applications of satellite-based AIS and for designing the next generation space-based AIS which might greatly improve the detection probability of ocean-going vessels. For example, one idea is to develop an AIS antenna with an innovative beam scanning method, which would scan the antenna across a wide swath to provide complete coverage and maintain the advantage of a narrow footprint to reduce signal collision (Cheng et al., 2015). At present, *TianTuo-3* is only an experimental satellite constellation. In the design, only one antenna is employed for receiving AIS signals. The results of this analysis show that even in the case of a single antenna, the detection probability of TT3-AIS for ocean-going vessels can be more than 40% and reaching up to about 80%, realising a comparatively high detection probability in ocean areas. However, the signal confliction problem for space-based AIS still requires further consideration, especially for offshore areas with dense traffic.

ACKNOWLEDGMENTS

This research has been supported by the National Natural Science Foundation of China under Grant No. 41004132 and 61302092, and the National University Defense Technology Project under Grant ZDYYJCYJ20140701.

REFERENCES

Brusch, S., Lehner, S., Schwarz, E. and Fritz, T. (2010). Near real time ship detection experiments. Advances in SAR Oceanography from ENVISAT, ERS and ESA third party missions, *Workshop ESA ESRIN, Frascati/Rome, Italy.*

Burzigotti, P., Ginesi, A. and Colavolpe, G. (2012). Advanced receiver design for satellite-based automatic identification system signal detection. *International Journal of Satellite Communications and Networking*, **30**, 52–63.

Cain, J.S. and Meger, E. (2009). Space-Based AIS: Contributing to Global Safety and Security. *Proceedings of the ISU 13th Annual Symposium, Strasbourg, France.*

Cairns, W.R. (2005). AIS and Long Range Identification & Tracking. *The Journal of Navigation*, **58**(2), 181–189.

Carson-Jackson, J. (2012). Satellite AIS – Developing Technology or Existing Capability? *The Journal of Navigation*, **65**, 303–321.

Carthel, C., Coraluppi, S., Grasso, R. and Grignan, P. (2007). Fusion of AIS, RADAR and SAR data for maritime surveillance - art. no. 67480Y[J]. *Proceedings of SPIE - The International Society for Optical Engineering,* 6748.

Cervera, M.A., Ginesi A. and Eckstein, K. (2011). Satellite-based vessel Automatic Identification System: A feasibility and performance analysis. *International Journal of Satellite Communications and Networking*, **29**, 117–142.

Chen, L.H., Chen, X.Q., Zhao, Y. and Cheng, Y. (2015). Design and on-orbit application of TT-1 satellite-based automatic identification system. *Journal of National University of Defense Technology*, **37**(1), 65–69 (in Chinese).

Cheng, Y., Chen, L.H. and Chen, X.Q. (2014). Modelling and simulation analysis of detection probability for space-based AIS. *Journal of National University of Defense Technology*, **36**(3), 51–57. (in Chinese)

Cheng, Y., Chen, L.H. and Chen, X.Q. (2015). A Beam Scanning Method based on the Helical Antenna for Space-based AIS. *Journal of Navigation*, **68**, 52–70.

Chaturvedi, S.K., Yang C., Ouchi K. and Shanmugam P. (2012). Ship recognition by integration of SAR and AIS. *Journal of Navigation*, **65**(2), 323–337.

Duffey, T., Huffine, C. and Nicholson, S. (2008). On-Orbit Results from the TacSat-2 ACTD Target Indicator Experiment AIS Payload. *Proceedings of the Symposium Small Satellites Systems & Services*, 660.

Eriksen, T., Høye, G., Narheim, B. and Meland, B.J. (2006). Maritime traffic monitoring using a space-based AIS receiver. *Acta Astronautica*, **58**(10), 537–549, http://dx.doi.org/10.1016/j.actaastro.2005.12.016.

Eriksen, T., Skauen, A., Narheim, B. and Helleren, Ø. (2010). Tracking ship traffic with space-based AIS: experience gained in first months of operations. *Proceedings of the Waterside Security Conference, Marina di Carrara, Italy*, doi: 10.1109/WSSC.2010.5730241.

ExactEarth. (2013). EV-1 Performance Review. http://www.exactearth.com/media-centre/past-issues-ofexact news/exactNews-Issue6.pdf.

Graveson, A. (2004). AIS–an inexact science. *The Journal of Navigation*, **57**, 339–343.

Holsten, S. (2009). Global maritime surveillance with satellite-based AIS. *In OCEANS 2009-Europe IEEE*.

Høye, G.K., Eriksen, T., Meland, B.J. and Narheim, B.T. (2008). Space-based AIS for global maritime traffic monitoring. *Acta Astronautica*, **62**(2), 240-245.

ITU. (2001). Technical Characteristics for a Universal Vessel-borne Automatic Identification System Using Time Division Multiple Access in the VHF Maritime Mobile Band. Technical Classifications of Recommendations ITU-M, 1371-1, Geneva, Switzerland.

ITU. (2010). Technical Classifications of Recommendations ITU-M.1371-4. Technical characteristics for an automatic identification system using time-division multiple access in the VHF maritime mobile band, Rec. ITU-R M.1371-4, 04/2010, 2010.

Li, S.Y., Chen, L.H. and Chen, X.Q. (2017a). Decoding analysis of the time information from the space-based AIS message. *Chinese Space Science and Technology,* **37**(1), 75–81, DOI: 10.16708/j.cnki.1000-758x.2017.0014. (in Chinese).

Li S.Y., Chen X.Q., Chen L.H., Zhao Y., Sheng T. and Bai Y.Z. (2017b). Data receiving analysis of the AIS on board the "TianTuo-3" Micro-satellite. *The Journal of Navigation*, **70**(4), 761–774.

Narheim, B., Helleren, O., Olsen, O., Olsen, R., Rosshaug, H., Beattie, A., Kekez, D. and Zee, R. (2011). Aissat-1 early results. 25th *Annual AIAA/USU Conference on Small Satellites, SSC11-III-6*. http://digitalcommons.usu.edu/smallsat/2011/all2011/26/

Silveira, P.A.M., Teixeira, A.P., and Guedes Soares, C. (2013). Use of AIS Data to Characterise Marine Traffic Patterns and Vessel Collision Risk off the Coast of Portugal. *The Journal of Navigation*, **66**, 879–898.

Skauen, A.N. (2016). Quantifying the tracking capability of space-based AIS systems. *Advances in Space Research*, **57**, 527–542, http://dx.doi.org/10.1016/j.asr.2015.11.028.

Tobehn, C., Schonenberg, A., Rinaldo, R., Ginesi, A., Ginati, A. and Sciberras, L. (2011). European Satellite AIS under Joint EMSA/ESA Integrated Applications Programme. *62nd International Astronautical Congress (IAC2011),* 1–10.

Vu Trong, T., Dinh Quoc, T., Dao Van, T., Pham Quang, H. and Nguyen, H. (2011). Constellation of small quick-launch and self-deorbiting Nano-satellites with AIS receivers for global vessel traffic monitoring. 2nd *Nano-Satellite Symposium, Tokyo, Japan.*

Wahl, T. and Høye, G. K. (2003). New Possible Roles of Small Satellites in Maritime Surveillance. *Proceedings of Fourth IAA Symposium on Small Satellites for Earth Observation, Berlin, Germany.*